

# The Payne Effect for Particle-Reinforced Elastomers

Aleksey D. Drozdov<sup>1</sup> and Al Dorfmann<sup>2</sup>

<sup>1</sup> *Institute for Industrial Mathematics, 4 Hanachtom Street*

*84311 Beersheba, Israel*

<sup>2</sup> *Institute of Structural Engineering, 82 Peter Jordan Street*

*1190 Vienna, Austria*

## Abstract

The study deals with the Payne effect (a substantial decrease in the storage modulus of a particle-reinforced elastomer with an increase in the amplitude of mechanical oscillations). The influence of temperature, concentration of filler and amplitude and frequency of strains is analyzed on the mechanical response of filled rubbery polymers. Constitutive equations are derived using the concept of two interpenetrating networks: one comprises semiflexible polymeric chains connected to temporary junctions, whereas the other is formed by aggregated filler clusters. Adjustable parameters are found by fitting experimental data for natural rubber, bromobutyl rubber and styrene-butadiene rubber reinforced by carbon black and polymeric particles. The critical concentration of particles is determined that characterizes transition from an ensemble of disjoint clusters to the network of filler. The volume fraction of filler corresponding to this transition is found to be close to theoretical predictions based on the percolation theory, as well as to experimental data for isolator-conductor transition.

## 1. Introduction

This paper is concerned with the Payne effect<sup>1–4</sup>: a noticeable decrease in the storage modulus of filled rubbery polymers with an increase in the amplitude of small-strain oscillations in dynamic mechanical tests. Changes in dynamic moduli of filled elastomers are traditionally associated with aggregation of filler particles into clusters and networks<sup>5–8</sup>. This phenomenon has attracted substantial attention of experimentalists in the past decade<sup>8–16</sup> because of its importance for industrial applications (airplane and automotive tires).

The strain-dependence of dynamic moduli is conventionally described in terms of the Kraus equations<sup>17</sup>

$$E' = E'_0 + \frac{\Delta E'}{1 + (\Delta/\Delta_0)^{2m}}, \quad E'' = E''_0 + \frac{\Delta E''(\Delta/\Delta_0)^m}{1 + (\Delta/\Delta_0)^{2m}}, \quad (1)$$

where  $E'$  and  $E''$  are storage and loss moduli in a dynamic test with the strain-amplitude  $\Delta$ ,  $E'_0$  and  $E''_0$  are dynamic moduli in a test with an infinitesimally small amplitude of strains, and  $\Delta_0$  and  $m$  are adjustable parameters. Equations (1) were developed with reference to the deagglomeration–reagglomeration mechanism for aggregation of filler clusters. The exponent  $m$  in Eqs. (1) is fairly well predicted in terms of the connectivity parameter for fractal aggregates<sup>6</sup>.

Formulas (1) provide an acceptable agreement with experimental data in dynamic tests with a fixed frequency of oscillations<sup>8,12</sup>. However, three shortcomings of the Kraus equations may be mentioned:

1. fitting observations for storage and loss moduli separately results in different values of adjustable parameters<sup>8,12</sup>;
2. Eqs. (1) do not describe changes in dynamic moduli of rubbery polymers with temperature, volume fraction of filler and frequency of oscillations;
3. the deagglomeration–reagglomeration concept does not distinguish between the response of an ensemble of disjoint clusters corresponding to small degrees of loading

and that for a filler network (an agglomerate superstructure<sup>15</sup>) observed in elastomers with high concentrations of reinforcing particles.

The neglect of the clusters–network transition implies that parameters of Eq. (1) smoothly change with the filler concentration. On the other hand, observations in dc conductivity tests reveal that conductivity of reinforced rubbery polymers increases by several orders of magnitude when the volume fraction of filler reaches some percolation threshold<sup>18–20</sup>. This contradiction implies the following questions: (i) whether an analog of the isolator–conductor transition is observed in dynamic mechanical tests, and (if so), (ii) whether the threshold concentrations of filler found in mechanical and dc conductivity experiments are close to one another.

We aim to develop a model which can correctly describe the effects of amplitude and frequency of oscillations on dynamic moduli. For this purpose we apply the theory of temporary polymeric networks<sup>21–24</sup> to characterize the time-dependent behavior of the host material and the concept of bound<sup>7,25</sup> and occluded<sup>5</sup> rubber to predict interactions between the elastomer and filler particles.

According to conventional theories of transient networks, a rubbery polymer is thought of as an incompressible network of long chains connected to temporary junctions. A chain whose ends are connected to separate junctions is treated as an active one. Snapping of an end of a chain from a junction is modeled as its breakage (transition from its active state to the dangling state). When a dangling chain captures a junction, a new active chain arises. Breakage and reformation of active chains (occurring at random times) are thought of as thermally activated processes.

Unlike previous studies where all chains are treated as composed of an identical number of strands, we suppose that chains contain various numbers of strands,  $n$ , and determine the distribution of chains by the probability density,  $p(n)$ , which is assumed to change with temperature, the volume fraction of filler and the strain intensity. To reduce the number of adjustable parameters in the governing equations, we adopt a discrete analog of the Gaussian

distribution,

$$p(n) = A \exp\left[-\frac{(n - N)^2}{2\Sigma^2}\right] \quad (n = 1, \dots, N_1), \quad p(n) = 0 \quad (n = N_1 + 1, \dots), \quad (2)$$

where  $N$  is the average number of strands in a chain,  $\Sigma$  is an analog of the standard deviation for the number of strands,  $N_1$  is the maximal number of strands in a chain, and the constant  $A$  is determined by the equality

$$\sum_{n=1}^{N_1} p(n) = 1.$$

The advantage of Eq. (2) is that given *a priori* quantities  $N$  and  $N_1$ , the distribution of chains is determined by the only parameter  $\Sigma$ .

Another refinement of the conventional theory of transient networks is that the rates of breakage and reformation for active chains are assumed to depend on the number of strands,  $n$ , which allows relaxation spectra of filled elastomers to be adequately predicted.

The theories of bound and occluded rubber presume that macro-strains in the host material are constrained by surrounding aggregates of filler. The theory of bound rubber, see Refs.<sup>20,25,26</sup> and the references therein, ascribes these constraints to adsorption of macromolecules on the filler surfaces, which results in formation of shells of the host material (with the thickness of about 10 nm<sup>20</sup>) around filler particles and their clusters. Physical properties of the surface layers are assumed to substantially differ from those for the unfilled elastomer<sup>27</sup>. In particular, elastic moduli and the resistance to the desorptive action of a solvent for the shells exceed those for the bulk polymer by several orders of magnitude<sup>19</sup>. NRM spectroscopy reveals an internal structure of the shells which consist of an inner domain of tightly bound macromolecules and an outer region of loosely bound chains<sup>20</sup>.

According to the concept of occluded rubber<sup>5</sup>, aggregation of isolated clusters of particles into a network results in separation of some meso-regions of the host material (occluded domains) from the bulk elastomer. When the filler network is relatively rigid, this implies shielding of constrained rubbery regions by the network which does not transmit stresses to the occluded regions. This results in strong inhomogeneity of macro-deformation. To

simplify the analysis, the host material is assumed to be split into meso-domains, in a part of which micro-strains coincide with the macro-strains in the sample, whereas in the other part micro-strains vanish.

The following scenario is proposed for deformation of a particle-reinforced elastomer. The distribution of chains,  $p(n)$ , in an unfilled rubbery polymer is characterized by a relatively small standard deviation  $\Sigma_0$  that determines its relaxation spectrum. For very small degrees of loading,  $\phi$ , the parameter  $\Sigma$  increases with the growth of the filler concentration which reflects creation of thin shells containing regions of loosely bound chains (the number of strands in chains belonging to these domains is assumed to differ from the “average” number for an unbounded rubber). For low concentrations of filler, when clusters do not aggregate into a network [the regime of disjoint clusters (DC)], changes in the viscoelastic response of a reinforced elastomer are associated with transformations occurring in surface layers around the filler particles and their flocks. We suppose that

1. given a temperature,  $T$ , and an amplitude of oscillations,  $\Delta$ , the quantity  $\Sigma$  decreases with the degree of loading  $\phi$  because of aggregation of isolated particles into clusters, whose surface area is substantially less than the sum of surface areas of separated particles;
2. given a degree of loading,  $\phi$ , and a strain amplitude,  $\Delta$ , the standard deviation of the number of strands,  $\Sigma$ , increases with temperature  $T$  because of a partial destruction of glassy-like shells of tightly linked chains around the filler particles and their clusters and transformation of tightly bound layers into loosely bound domains;
3. given a temperature,  $T$ , and a degree of loading,  $\phi$ , the parameter  $\Sigma$  weakly decreases with the amplitude of oscillations  $\Delta$  because of mechanically induced breakage of long chains in the regions of loosely bound rubber and their subsequent amalgamation with the host elastomer.

At high concentrations of filler, when clusters of reinforcing particles are aggregated into a

network [the regime of network rupture (NR)], changes in the time-dependent response of a rubbery polymer are mainly determined by interactions between the host material and the network. We suppose that

1. given a temperature,  $T$ , and an amplitude of oscillations,  $\Delta$ , the quantity  $\Sigma$  strongly decreases with the degree of loading  $\phi$  because of coalescence of flocks into a fractal network, which causes a noticeable reduction in the lateral surface of clusters to which regions of loosely bound rubber are adjusted;
2. given a degree of loading,  $\phi$ , and a strain amplitude,  $\Delta$ , the standard deviation of the number of strands,  $\Sigma$ , decreases with temperature  $T$  because of the growth of rate of breakage for long chains in the regions of loosely bound rubber and their subsequent merging with the bulk polymer;
3. given a temperature,  $T$ , and a degree of loading,  $\phi$ , the quantity  $\Sigma$  dramatically decreases with the amplitude of oscillations  $\Delta$  because of mechanically induced rupture of the filler network and its crumbling into separated clusters.

The objective of this study is to validate this scenario by comparing results of numerical simulation with available experimental data. The exposition is organized as follows. Section 2 deals with the kinetics of rearrangement for a temporary network of long chains. Stress-strain relations for a transient polymeric network are derived in Section 3. The constitutive equations are applied to describe uniaxial extension of a specimen in Section 4. Section 5 is concerned with comparison of experimental data for filled rubbery polymers with results of numerical simulation. Some concluding remarks are formulated in Section 6.

## **2. Rearrangement of a temporary network**

The distribution of chains in a polymeric network is determined by the total number of active chains per unit mass,  $\Xi$ , and the probability density of long chains composed of  $n$  strands,  $p(n)$ . We focus on the stationary response of filled elastomers in dynamic mechanical

tests with small strains and assume that the quantities  $\Xi$  and  $p(n)$  are independent of time (however, these parameters may, in general, depend on the amplitude of oscillations).

Denote by  $X(t, \tau, n)$  the number of active chains with  $n$  strands (per unit mass) at time  $t$  that has last been linked to the network at instant  $\tau \in [0, t]$ . The function  $X(t, \tau, n)$  entirely determines the current state of a polymeric network:

$$X(t, t, n) = \Xi p(n) \tag{3}$$

equals the number of active chains (per unit mass) with  $n$  strands at time  $t$ ;

$$\left. \frac{\partial X}{\partial \tau}(t, \tau, n) \right|_{t=\tau} d\tau$$

is the number of active chains with  $n$  strands (per unit mass) that have merged with the network within the interval  $[\tau, \tau + d\tau]$ ;

$$\frac{\partial X}{\partial \tau}(t, \tau, n) d\tau$$

is the number of these chains that did not break during the interval  $[\tau, t]$ ;

$$-\frac{\partial X}{\partial t}(t, 0, n) dt$$

is the number of active chains (per unit mass) that detach from the network (for the first time) within the interval  $[t, t + dt]$ , and

$$-\frac{\partial^2 X}{\partial t \partial \tau}(t, \tau, n) dt d\tau$$

is the number of chains (per unit mass) that has last been linked to the network within the interval  $[\tau, \tau + d\tau]$  and detach from the network (for the first time after merging) during the interval  $[t, t + dt]$ .

The kinetics of reformation is determined by the relative rate of breakage for active chains,  $\Gamma(n)$ , and by the rate of merging of dangling links with the network,  $\gamma(n)$ . The relative rate of breakage is defined as the ratio of the number of active chains broken per unit time to the total number of active chains,

$$\Gamma(n) = -\frac{1}{X(t, 0, n)} \frac{\partial X}{\partial t}(t, 0, n) = -\left[\frac{\partial X}{\partial \tau}(t, \tau, n)\right]^{-1} \frac{\partial^2 X}{\partial t \partial \tau}(t, \tau, n). \quad (4)$$

The rate of breakage  $\Gamma$  may, in general, depend on the current time  $t$ , on the instant  $\tau$  when a chain has been last bridged to the network and on the guiding vector  $\mathbf{l}$  (the unit vector whose direction coincides with the end-to-end vector  $\mathbf{R}$  of the chain at time  $\tau$ ). The neglect of these dependences means that the network is homogeneous (the rate of breakage for a chain is independent of the instant of its connection to the network,  $\tau$ , and on the current time,  $t$ ) and isotropic (the rate of breakage is independent of the chain direction at the instant of merging). For a homogeneous and isotropic network, the rate of merging,  $\gamma$ , is independent of the instants  $t$  and  $\tau$ , as well as of the vector  $\mathbf{l}$ . It is defined as the number of dangling chains (per unit mass) bridged to the network per unit time,

$$\gamma(n) = \left. \frac{\partial X}{\partial \tau}(t, \tau, n) \right|_{\tau=t}. \quad (5)$$

Integration of differential equations (4) with the initial conditions (3) and (5) implies that

$$X(t, 0, n) = \Xi p(n) \exp[-\Gamma(n)t], \quad \frac{\partial X}{\partial \tau}(t, \tau, n) = \gamma(n) \exp[-\Gamma(n)(t - \tau)]. \quad (6)$$

Because the total number of active chains remains time-independent, the number of broken chains coincides with the number of reformed chains

$$\gamma(n) = -\frac{\partial X}{\partial t}(t, 0, n) - \int_0^t \frac{\partial^2 X}{\partial t \partial \tau}(t, \tau, n) d\tau.$$

Substitution of Eq. (6) into this equality implies the balance law

$$\gamma(n) = \Gamma(n) \left\{ \Xi p(n) \exp[-\Gamma(n)t] + \gamma(n) \int_0^t \exp[-\Gamma(n)(t - \tau)] d\tau \right\}.$$

The solution of this equation reads

$$\gamma(n) = \Xi \Gamma(n) p(n). \quad (7)$$

Equations (6) and (7) entirely determine the current state for a temporary network of long chains.



### 3. Constitutive relations for a transient network

The stress in a dangling chain is assumed to totally relax before this chain captures a new junction, which implies that the natural (stress-free) state of an active chain coincides with the deformed state of the network at the instant of their merging. The extension ratio for a chain bridged to the network at time  $\tau$  and not broken within the interval  $[\tau, t]$  reads<sup>28</sup>

$$\lambda(t, \tau, \mathbf{l}) = [\mathbf{l} \cdot \mathbf{C}(t, \tau) \cdot \mathbf{l}]^{\frac{1}{2}},$$

where  $\mathbf{C}(t, \tau)$  is the relative Cauchy deformation tensor for transition from the deformed state of the network at time  $\tau$  to the deformed state at time  $t$  and the dot stands for inner product. At small strains, this equality implies that

$$\varepsilon(t, \tau, \mathbf{l}) = \mathbf{l} \cdot \mathcal{E}(t, \tau) \cdot \mathbf{l}, \quad \mathcal{E}(t, \tau) = \epsilon(t) - \epsilon(\tau), \quad (8)$$

where  $\varepsilon = \lambda - 1$  is the longitudinal strain for a chain,  $\mathcal{E} = \frac{1}{2}(\mathbf{C} - \mathbf{I})$  is the relative Cauchy strain tensor for the network,  $\mathbf{I}$  is the unit tensor and  $\epsilon(t)$  is the strain tensor for transition from the stress-free state of the network to its deformed state at time  $t$ . By analogy with the Kratky–Porod model, we suppose that strains in all strands coincide, which implies that the strain per strand equals  $\varepsilon/n$  for a chain comprising  $n$  strands. Modeling strands as linear elastic solids with a constant rigidity  $\mu$ , we find the mechanical energy of a chain,

$$\frac{1}{2} \sum_{i=1}^n \mu \left( \frac{\varepsilon}{n} \right)^2 = \mu \frac{\varepsilon^2}{2n}.$$

With reference to the conventional assumption that the excluded-volume effect and other multi-chain effects are screened for an individual chain by surrounding macromolecules, we neglect the energy of interaction between chains and calculate the mechanical energy of a network as the sum of the mechanical energies for individual chains. The mechanical energy (per unit mass) of initial chains which have not been broken within the interval  $[0, t]$  is given by

$$\frac{1}{4\pi} \sum_{n=1}^{\infty} \frac{\mu}{2n} X(t, 0, n) \int_S \varepsilon^2(t, 0, \mathbf{l}) dA(\mathbf{l}), \quad (9)$$

where  $\mathcal{S}$  is the unit sphere in the space of vectors  $\mathbf{l}$  and  $dA(\mathbf{l})$  is the surface element on  $\mathcal{S}$ . The mechanical energy (per unit mass) of chains that merged with the network within the interval  $[\tau, \tau + d\tau]$  and are connected with the network until the current time  $t$  reads

$$\frac{1}{4\pi} \sum_{n=1}^{\infty} \frac{\mu}{2n} \frac{\partial X}{\partial \tau}(t, \tau, n) d\tau \int_{\mathcal{S}} \varepsilon^2(t, \tau, \mathbf{l}) dA(\mathbf{l}). \quad (10)$$

To calculate the integrals over  $\mathcal{S}$ , we introduce a Cartesian coordinate frame  $\{x_i\}$  whose base vectors  $\mathbf{k}_i$  are directed along the eigenvectors of the symmetrical tensor  $\mathcal{E}$ :

$$\mathcal{E} = \mathcal{E}_1 \mathbf{k}_1 + \mathcal{E}_2 \mathbf{k}_2 + \mathcal{E}_3 \mathbf{k}_3,$$

where  $\mathcal{E}_i$  is the  $i$ th eigenvalue of the tensor  $\mathcal{E}$ . The position of the unit vector  $\mathbf{l}$  with respect to the coordinate frame is determined by the Euler angles  $\varphi$  and  $\vartheta$ ,

$$\mathbf{l} = \sin \vartheta (\cos \varphi \mathbf{k}_1 + \sin \varphi \mathbf{k}_2) + \cos \vartheta \mathbf{k}_3.$$

Substitution of these expressions into Eq. (8) results in

$$\varepsilon = \sin^2 \vartheta (\mathcal{E}_1 \cos^2 \varphi + \mathcal{E}_2 \sin^2 \varphi) + \mathcal{E}_3 \cos^2 \vartheta.$$

Bearing in mind that  $dA = \sin \vartheta d\vartheta d\varphi$ , we obtain

$$\begin{aligned} \int_{\mathcal{S}} \varepsilon^2 dA &= \int_0^\pi \sin \vartheta d\vartheta \int_0^{2\pi} \left[ \sin^2 \vartheta (\mathcal{E}_1 \cos^2 \varphi + \mathcal{E}_2 \sin^2 \varphi) + \mathcal{E}_3 \cos^2 \vartheta \right]^2 d\varphi \\ &= \frac{4\pi}{15} \left[ 3(\mathcal{E}_1^2 + \mathcal{E}_2^2 + \mathcal{E}_3^2) + 2(\mathcal{E}_1 \mathcal{E}_2 + \mathcal{E}_1 \mathcal{E}_3 + \mathcal{E}_2 \mathcal{E}_3) \right]. \end{aligned}$$

Summing expressions (9) and (10) and using this equality, we arrive at the formula for the strain energy density of the network (per unit mass)

$$\begin{aligned} U(t) &= \frac{\mu}{30} \sum_{n=1}^{\infty} \left\{ X(t, 0, n) \left[ 3I_1^2(\mathcal{E}(t, 0)) - 4I_2(\mathcal{E}(t, 0)) \right] \right. \\ &\quad \left. + \int_0^t \frac{\partial X}{\partial \tau}(t, \tau, n) \left[ 3I_1^2(\mathcal{E}(t, \tau)) - 4I_2(\mathcal{E}(t, \tau)) \right] d\tau \right\}, \end{aligned}$$

where  $I_i$  stands for the  $i$ th principal invariant of a tensor. It follows from this equality, the incompressibility condition,  $I_1(\mathcal{E}) = 0$ , and Eq. (8) that

$$U(t) = -\frac{2\mu}{15} \sum_{n=1}^{\infty} \frac{1}{n} \left[ X(t, 0, n) I_2(\epsilon_d(t)) + \int_0^t \frac{\partial X}{\partial \tau}(t, \tau, n) I_2(\epsilon_d(t) - \epsilon_d(\tau)) d\tau \right], \quad (11)$$

where  $\epsilon_d$  is the deviatoric part of the strain tensor  $\epsilon$ . The deviatoric component  $\sigma_d$  of the stress tensor  $\sigma$  is determined by the conventional relationship

$$\sigma_d(t) = \rho \frac{\partial U(t)}{\partial \epsilon_d(t)},$$

where  $\rho$  is mass density. Substitution of Eqs. (6), (7) and (11) into this equality results in the stress-strain relation

$$\begin{aligned} \sigma(t) = & -P(t)\mathbf{I} + \frac{2}{15} \mu \rho \Xi \sum_{n=1}^{\infty} \frac{p(n)}{n} \left[ \exp(-\Gamma(n)t) \epsilon_d(t) \right. \\ & \left. + \Gamma(n) \int_0^t \exp(-\Gamma(n)(t-\tau)) (\epsilon_d(t) - \epsilon_d(\tau)) d\tau \right], \end{aligned} \quad (12)$$

where  $P$  is pressure.

#### 4. Uniaxial extension of a network

For uniaxial extension of an incompressible network along the axis  $x_1$  of the Cartesian coordinate frame  $\{x_i\}$ , the strain tensor reads

$$\epsilon(t) = \epsilon(t) [\mathbf{k}_1 \mathbf{k}_1 - \frac{1}{2} (\mathbf{k}_2 \mathbf{k}_2 + \mathbf{k}_3 \mathbf{k}_3)],$$

where  $\epsilon(t)$  is the longitudinal strain. Substitution of this equality into Eq. (12) results in the formula for the longitudinal stress  $\sigma(t)$ ,

$$\sigma(t) = \frac{1}{5} \mu \rho \Xi \sum_{n=1}^{\infty} \frac{p(n)}{n} \left[ \epsilon(t) - \Gamma(n) \int_0^t \exp(-\Gamma(n)(t-\tau)) \epsilon(\tau) d\tau \right]. \quad (13)$$

We now aim to establish a correspondence between the longitudinal strain for the network,  $\epsilon(t)$ , and the macro-strain for a specimen,

$$e(t) = \frac{L(t) - L(0)}{L(0)}, \quad (14)$$

where  $L(t)$  is the current length of a specimen. At low concentrations of filler (the DC regime), we assume that the host material is homogeneous and postulate that the micro-strains in active chains coincide with the macro-strain in the specimen,

$$\epsilon(t) = e(t). \quad (15)$$

At high degrees of loading (the NR regime), deformation of a part of the rubbery polymer is assumed to be screened by the network. To describe restrictions imposed by the filler network on deformation of a reinforced elastomer, we (i) postulate that the network is rigid and (ii) characterize the level of constraints by the volume fraction of the undeformed host material. For uniaxial loading, this fraction is uniquely determined by the length,  $L_0(t)$ , of a part of the sample occupied by occluded rubber. Under the hypothesis that deformation in the rest of the specimen is homogeneous, we find the longitudinal elongation for the unconstrained part of the bulk material as the ratio of the current length of this part to its initial length,

$$\lambda_*(t) = \frac{L(t) - L_0(t)}{L(0) - L_0(t)}.$$

We substitute Eq. (14) into this equality, introduce the longitudinal strain by the conventional formula,  $e_* = \lambda_* - 1$ , neglect terms of the second order of smallness compared with  $e(t)$ , and postulate that the micro-strains in long chains coincide with the macro-strain in the unrestricted part of the rubbery polymer. This implies that

$$\epsilon(t) = \frac{L(0)}{L(0) - L_0(t)} e(t). \quad (16)$$

When the filler network is absent,  $L_0(t) = 0$ , and Eq. (16) turns into Eq. (15). A similar equality was proposed in Ref.<sup>30</sup> based on the concept of the strain-amplification factor. Unlike previous studies, where the coefficient on the right-hand side of Eq. (16) was expressed in terms of the filler concentration and the ratio of the average length to the average width of chain-like filler clusters by using a phenomenological equation, we do not concretize the shape of the function  $L_0(t)$  and determine it by fitting observations. As will be demonstrated in Section 5, this function strongly depends on the strain intensity, which implies that treatment of  $L_0$  as a function of the volume fraction of filler is an oversimplification.

For a dynamic test with an amplitude  $\Delta$  and a frequency  $\omega$ , we set

$$e(t) = \Delta \exp(i\omega t), \quad (17)$$

where  $i = \sqrt{-1}$ . Combining Eqs. (13), (16) and (17) and introducing the new variable  $s = t - \tau$ , we find that

$$E^*(t, \omega) = K_0(t) \sum_{n=1}^{\infty} \frac{p(n)}{n} \left[ 1 - \Gamma(n) \int_0^t \exp(-(\Gamma(n) + i\omega)s) \frac{L(0) - L_0(t)}{L(0) - L_0(t-s)} ds \right],$$

where

$$E^*(t, \omega) = \frac{\sigma(t)}{e(t)}$$

is the complex modulus and  $K_0(t) = \frac{1}{5}\mu\rho\Xi L(0)[L(0) - L_0(t)]^{-1}$ .

It is natural to assume that under periodic loading, the function  $L_0(t)$  rapidly approaches its limiting value  $L_\infty(\Delta)$  corresponding to the steady-state regime of oscillations. Replacing the function  $L_0(t)$  by the constant  $L_\infty(\Delta)$ , putting  $t = \infty$  as the upper limit of integration, and splitting  $E^*$  into the sum

$$E^* = E' + iE'',$$

where  $E'(\omega)$  is the storage modulus and  $E''(\omega)$  is the loss modulus, we arrive at the formulas

$$E'(\omega) = K\omega^2 \sum_{n=1}^{\infty} \frac{p(n)}{n[\Gamma^2(n) + \omega^2]}, \quad E''(\omega) = K\omega \sum_{n=1}^{\infty} \frac{p(n)\Gamma(n)}{n[\Gamma^2(n) + \omega^2]} \quad (18)$$

with

$$K = \frac{1}{5}\mu\rho\Xi \frac{L(0)}{L(0) - L_\infty}. \quad (19)$$

Given quantities  $N$  and  $N_1$ , Eqs. (18) are determined by two adjustable parameters,  $K$  and  $\Sigma$ , and the rate of slippage from temporary junctions,  $\Gamma(n)$ . To reduce the number of constants to be found, we set

$$\Gamma(n) = \Gamma_0 n^\kappa, \quad (20)$$

where  $\Gamma_0$  and  $\kappa$  are positive parameters. To explain the increase in the rate of breakage for active chains with the number of strands, we assume that chains have finite bending stiffness. A semiflexible chain is treated as a curvilinear rod whose micro-motion is confined

to some tube formed by surrounding macromolecules<sup>29</sup>. When the rod has a negligible bending rigidity, lateral oscillations driven by thermal fluctuations have a local character, which implies that slippage of a chain end from a junction is induced by random excitations occurring (rather sparsely) in the close vicinity of this end. For a rod with a finite bending rigidity, lateral oscillations induce transverse waves, whose amplitudes increase because of their interaction with end-points. The amplification of random transverse oscillations of an elastic rod in the vicinity of its end-points results in the growth of the rate of slippage of chain ends from temporary junction. The account for finite bending stiffness of semiflexible chains allows the monotonic growth of the function  $\Gamma(n)$  to be explained. It does not, however, result in the power-law dependence (20), which is treated as purely phenomenological.

## 5. Comparison with experimental data

We begin with fitting observations in dynamic tensile tests for a carbon black (CB) filled natural rubber vulcanizate with the degree of loading  $\phi = 50$  phr (parts per hundred parts of rubber) at various temperatures  $T$ . For a detailed description of specimens and the experimental procedure, see Ref.<sup>13</sup>. To approximate experimental data, we set  $N = 40$ , which is in qualitative agreement with the average number of strands used in other studies (for example,  $N = 12$  was assumed for glassy styrene-acrylonitrile polymer<sup>31</sup> and  $N = 20$  was employed in molecular dynamics simulations of interactions between a polymeric melt and filler particles<sup>32</sup>), and  $N_1 = 500$ . Numerical analysis demonstrates that changes in the values of  $N$  and  $N_1$  (in the range from  $N = 30$  to  $N = 50$  and from  $N_1 = 100$  to  $N_1 = 1000$ ) weakly affect the quality of fitting.

At any temperature  $T$ , we, first, fit the curves  $E'(\omega)$  measured at the minimum amplitude of oscillations,  $\Delta_{\min} = 0.006$ , and determine parameters  $\Gamma_0$ ,  $\kappa$  and  $\Sigma$  (by the steepest-descent procedure) which ensure the best quality of matching. Afterwards, we fix the values of these quantities and approximate observations by using only one adjustable parameter,  $K$ , which is determined by the least-squares algorithm. Figures 1 demonstrate fair agreement between

experimental data and results of numerical simulation.

The independence of the standard deviation of the number of strands,  $\Sigma$ , from the amplitude of oscillations,  $\Delta$ , implies that the viscoelastic response of the filled rubber corresponds to the DC regime (low degrees of loading) at all temperatures  $T$ .

The elastic modulus  $K$  is plotted versus the amplitude of oscillations  $\Delta$  in Figure 2A which demonstrates that the modulus slowly decreases with the strain amplitude. Experimental data are fairly well approximated by the function

$$\log K = a_0 - a_1 \Delta, \quad (21)$$

where adjustable parameters  $a_i$  are found by the least-squares technique. According to Eq. (19), below the cluster–network transition point, the modulus  $K$  is proportional to the number of active chains per unit mass,  $\Xi$ . A decrease in  $K$  with  $\Delta$  means that the growth of strains results in a reduction of the number of active chains because of the mechanically induced agitation of the breakage process. This conclusion is in agreement with observations for unfilled rubbery polymers<sup>28</sup>.

The quantities  $\Sigma$  and  $a_0 = \log K(0)$  (the logarithm of the elastic modulus  $K$  for the infinitesimally small amplitude of oscillations) are plotted in Figure 2B versus the degree of undercooling,  $\Delta T = T - T_g$ , where  $T_g$  is the glass transition temperature. Experimental data are approximated by the functions

$$\log \Sigma = b_0 - \frac{b_1}{\Delta T}, \quad \log K(0) = c_0 + \frac{c_1}{\Delta T}, \quad (22)$$

where the parameters  $b_i$  and  $c_i$  are found by the least-squares algorithm. Equations (22) provide good fitting of observations. An increase in the standard deviation of the number of strands  $\Sigma$  with temperature is in agreement with the proposed mechanism for transformation of the tightly bound domains into the loosely bound regions. A decrease in the elastic modulus with temperature confirms the hypothesis about the elastic nature of the response of long chains (according to the conventional theory of entropic elasticity, the modulus linearly increases with temperature because of the growth in the number of available configurations

for long chains<sup>33</sup>). Equations (19) and (22) imply that the rigidity of strands,  $\mu$ , decreases with temperature.

The rate of breakage for active chains  $\Gamma_0$  is plotted versus the degree of undercooling in Figure 2C, which demonstrates that  $\Gamma_0$  monotonically decreases with temperature and reaches its limiting value,  $\Gamma_\infty$ , at high temperatures. Experimental data are approximated by the phenomenological relation

$$\log \Gamma_0 = d_0 - d_1 \Delta T \quad (23)$$

with adjustable parameters  $d_i$ .

At first glance, the decrease in the rate of breakage with temperature is rather surprising, because the growth of temperature should result in an increase in the rate of thermally activated processes. Observations depicted in Figure 2C may be adequately explained, however, in the framework of the model of transient networks of semiflexible chains. The growth of temperature implies, on the one hand, an increase in the rate of thermal fluctuations which intensifies the breakage process. On the other hand, it induces a decrease in the bending rigidity of elastic chains, which means that transverse oscillations driven by thermal fluctuations at intermediate points of a chain are not transmitted to its ends, and, as a consequence, their amplitudes do not grow because of interactions of bending waves with the end-points.

The parameter  $\kappa$  that describes the influence of the length of an active chain on its rate of rearrangement is depicted in Figure 2D as a function of temperature  $T$ . The quantity  $\kappa$  increases with  $T$  at relatively low temperatures and becomes practically constant at elevated temperatures.

We proceed with fitting observations in dynamic tensile tests at room temperature for CB filled bromobutyl rubber. A detailed description of specimens and the experimental procedure is given in Ref.<sup>9</sup>. To reduce the number of adjustable parameters, we fix the average number of strands in a chain (the same as for the CB filled natural rubber),  $N = 40$ , and set  $N_1 = 80$  (which implies the symmetry of the probability density  $p(n)$  with respect to the point  $N$ ). Matching observations in a tensile test with the minimum amplitude of



oscillations  $\Delta_{\min} = 0.0003$  results in  $\Gamma_0 = 0.0088 \text{ s}^{-1}$ . We fix this value and approximate experimental data in other tests with the help of the adjustable parameters  $\kappa$ ,  $\Sigma$  and  $K$ . For any degree of loading,  $\phi$ , we determine the parameter  $\kappa$  by fitting the curve  $E'(\omega)$  measured at the minimum amplitude of strains,  $\Delta_{\min}$ . Afterwards, we fix the value of  $\kappa$  and match observations in dynamic tests with other amplitudes of oscillations by using only two adjustable parameters,  $\Sigma$  and  $K$ . The quantity  $\Sigma$  is determined using the steepest-descent procedure and the constant  $K$  is found by the least-squares algorithm. Figure 3 demonstrates fair agreement between experimental data and results of numerical simulation.

The parameters  $\Sigma$  and  $K$  are plotted versus the amplitude of oscillations  $\Delta$  in Figure 4. Experimental data are fairly well approximated by the functions

$$\log \Sigma = A_0 - A_1 \log \Delta, \quad \log K = B_0 + B_1 \log \Delta, \quad (24)$$

where the parameters  $A_i$  and  $B_i$  are determined using the least-squares algorithm.

Two different regimes in the material behavior are revealed. At small amplitudes,  $\Delta < \Delta_{\text{cr}}$ ,  $\Sigma$  and  $K$  weakly change with  $\Delta$  (curves 1). The standard deviation of the number of strands decreases at the minimum degree of loading,  $\phi = 30$  phr, and remains practically constant for  $\phi \geq 50$  phr. The elastic modulus  $K$  increases with  $\Delta$  at  $\phi \leq 50$  phr and decreases at  $\phi > 50$  phr. These changes may be associated with transition of bound rubber from the tight state to the loose state. At large amplitudes,  $\Delta > \Delta_{\text{cr}}$ ,  $\Sigma$  monotonically decreases and  $K$  strongly increases with  $\Delta$  (curves 2), which may be explained by disintegration of the filler network and release of occluded rubber.

The parameters  $A_0$  and  $A_1$  corresponding to the post-fracture regime for the filler network are plotted versus the degree of loading  $\phi$  in Figure 5A. Analogous dependences for the sub-fracture regime are not presented because of the insufficient number of experimental data for the parameter  $\Sigma$  (the best fit of observations depicted in Figures 4C and 4D is reached for the homogeneous distribution of chains with various numbers of strands). Experimental data in Figure 5A are fairly well approximated by the functions

$$A_0 = A_{00} + A_{01}\phi, \quad A_1 = A_{10} - A_{11}\phi \quad (25)$$

where adjustable parameters  $A_{ij}$  are found by the least-squares method. It follows from Eqs. (24) and (25) that in the interval of strains under consideration, the standard deviation of the number of strands decreases with the filler concentration, in agreement with the proposed scenario (at high volume fractions of filler, aggregation of clusters into a network results in a decrease in the number of isolated particles, and, as a consequence, in a decrease in the number of chains belonging to the surface layers).

The parameter  $B_0$  and  $B_1$  for the sub-fracture regime for the filler network are depicted in Figure 5B versus the degree of loading  $\phi$ . Experimental data are correctly predicted by the functions

$$B_0 = B_{00} - B_{01}\phi, \quad B_1 = B_{10} - B_{11}\phi, \quad (26)$$

where adjustable parameters  $B_{ij}$  are determined by the least-squares algorithm. Because the quantities  $B_0$  and  $B_1$  remain practically constant in the post-fracture regime, appropriate figures for these parameters are omitted.

Results presented in Figures 5A and 5B may be treated as a confirmation of the model because they reveal a plausible (from the physical standpoint) behavior of adjustable parameters in the constitutive equations with changes in the filler concentration.

The critical amplitude of oscillations  $\Delta_{\text{cr}}$  corresponding to fracture of the filler network is plotted in Figure 5C versus the degree of loading  $\phi$ . Observations are fairly well approximated by the function

$$\Delta_{\text{cr}} = C(\phi - \phi_{\text{cr}})^{-\beta}, \quad (27)$$

where the parameters  $C$ ,  $\beta$  and  $\phi_{\text{cr}}$  are found by the steepest-descent procedure. Following Ref.<sup>8</sup>, we find that the critical loading  $\phi_{\text{cr}} = 41$  prh corresponds to the critical volume fraction  $\psi_{\text{cr}} = 0.154$ , which is rather close to the theoretical percolation threshold  $\psi_* = 0.18$  for a spatial network of hard spheres<sup>34</sup>, as well as to the critical volume fraction  $\psi_* = 0.14$  for the isolator-conductor transition for CB natural rubber determined in dc conductivity tests<sup>18</sup>. The exponent  $\beta = 0.662$  in Eq. (27) is also in good agreement with the theoretical

predictions  $\beta_* = 0.70 \pm 0.02$ , see Ref.<sup>35</sup>, and  $\beta_* = 0.72$ , see Ref.<sup>18</sup>. Our estimate for the critical loading is confirmed by observations depicted in Figures 4A and 4B, which reveal that transition from the DC regime to the NR regime occurs at the degree of loading,  $\phi$ , belonging to the interval between 30 and 50 phr.

The exponent  $\kappa$  is plotted versus the degree of loading  $\phi$  in Figure 5D, which demonstrates that the parameter  $\kappa$  (which characterizes the rate of breakage for long chains) remains constant for the NR regime.

To assess the effect of temperature  $T$  on the distribution of long chains, we fit experimental data for the CB filled bromobutyl rubber in dynamic tensile tests at the temperatures  $T = 25$ ,  $T = 50$  and  $T = 100$  °C. The amplitude of strain oscillations  $\Delta = 0.01$  corresponds to the regime of rupture for the filler network. Figures 6A and 6B demonstrate fair agreement between observations and results of numerical analysis with  $N = 40$ ,  $N_1 = 80$  and  $\kappa = 16.0$ . In matching experimental data at various temperatures, the parameter  $\Gamma_0$  is treated as an adjustable parameter. Surprisingly, it is found that its value that ensures the best fit of experimental data is independent of temperature and equals  $\Gamma_0 = 0.0088 \text{ s}^{-1}$ .

The standard deviation of the number of strands,  $\Sigma$ , and the elastic modulus  $K$  are depicted in Figures 6C and 6D versus the degree of undercooling,  $\Delta T$ . Observations are approximated by the functions (22) used to match experimental data for the CB filled natural rubber in the DC regime. Comparison of Figure 2B with Figures 6C and 6D implies that the materials under consideration demonstrate different behavior for the DC and NR regimes. In the regime of disjoint clusters, the growth of temperature results in an increase in  $\Sigma$  and a decrease in  $K$ . On the contrary, in the regime of network rupture, the standard deviation of the number of strands decreases and the elastic modulus increases with temperature. The rates of changes in these parameters increase with the volume fraction of filler which may serve as a measure of connectivity for the network. The difference in the material response observed in these figures is in agreement with the proposed scenario for mechanically induced changes in the micro-structure of filled elastomers.

Finally, we approximate observations for styrene-butadiene rubber filled by carbon black

and polymeric particles in dynamic shear tests with the strain amplitude  $\Delta = 0.002$  at the temperature  $T = -30$  °C. A detailed description of specimens and the experimental procedure is found in Ref.<sup>8</sup>. Our aim is to assess the influence of the filler material on adjustable parameters in the constitutive equations.

Figures 7A and 7B demonstrate fair agreement between experimental data and results of numerical simulation with  $N = 40$ ,  $N_1 = 80$ ,  $\Gamma_0 = 0.0012 \text{ s}^{-1}$  and  $\kappa = 4.33$ . The quantities  $\Sigma$  and  $K$  are depicted versus the degree of loading  $\phi$  in Figures 7C and 7D. Observations are fairly well approximated by the functions

$$\log \Sigma = C_0 + C_1\phi, \quad \log K = D_0 - D_1\phi, \quad (28)$$

where the constants  $C_i$  and  $D_i$  are determined by the least-squares technique. Figure 7 reveals transition from the DC regime of micro-structural changes at small concentrations of filler to the NR regime at large degrees of loading. The critical concentration reads  $\phi_{\text{cr}} \approx 40$  phr for CB particles and  $\phi_{\text{cr}} \approx 30$  phr for polymeric particles. For the DC regime, the standard deviation of the number of strands,  $\Sigma$ , slowly changes with  $\phi$  (increases for the polymeric filler and decreases for the CB filler, in agreement with data depicted in Figure 4A), whereas the elastic modulus  $K$  increases with  $\phi$  for both kinds of filler (in agreement with observations presented in Figure 4A). For the NR regime, the quantity  $\Sigma$  increases and the modulus  $K$  decreases with  $\phi$  for both kinds of filler. It is worth noting that the rates of changes in  $\Sigma$  and  $K$  with the degree of loading are similar for CB and polymeric particles. This means that in the regime of disintegration of the filler network, the viscoelastic response of filled elastomers is mainly determined by the topological properties of the network and it rather weakly depends on physical properties of the reinforcement.

## 6. Concluding remarks

Constitutive equations have been derived for the mechanical response of particle-reinforced elastomers at small strains. The model is applied to describe the Payne effect: changes in the dynamic moduli of filled rubbery polymers with an increase in the amplitude of

strain-oscillations. The viscoelastic behavior of reinforced rubbers demonstrates two different regimes associated with (i) transformations of bound rubber in the close vicinity of filler particles and their clusters and (ii) fracture of the filler network and its disintegration into disjoint clusters of particles. The critical concentration of filler corresponding to the transition from the DC regime to the NR regime is in good agreement with theoretical predictions by the percolation theory, as well as with experimental data for dc conductivity.

The following conclusions are drawn:

1. Constitutive equations correctly predict observations in dynamic mechanical tests on filled elastomers at various temperatures, filler concentrations, amplitudes and frequencies of oscillations.
2. Changes in conditions of mechanical experiments result in changes in adjustable parameters of the model which are adequately described within the concepts of bound and occluded rubber and which are in agreement with the proposed scenario for transition from the DC regime to the NR regime of deformation.

The work is confined to the effects of temperature, filler concentration and amplitude and frequency of strain oscillations on the viscoelastic response of filled rubbers. Some important questions, however, remain beyond the scope of this study. They include, in particular, (i) the influence of the shape of particles, the distribution of their sizes<sup>36</sup>, and the presence of coupling agents<sup>10</sup> on the rheology of reinforced elastomers, (ii) changes in the glass transition temperature of filled rubbery polymers caused by polymer–filler interactions, as well as (iii) the effect of mechanical loading on electrical conductivity of reinforced elastomers<sup>37,38</sup>. These issues will be the subject of a subsequent publication.

## ACKNOWLEDGMENTS

Partial support from the European Commission under contract No. G1RD–CT–1999–00085 is gratefully acknowledged. AD acknowledges financial support by the Israeli Ministry of

Science through grant 1202-1-00.

## REFERENCES

1. A.R. Payne, *J. Appl. Polym. Sci.* **6**, 57, 368 (1962).
2. A.R. Payne, *J. Appl. Polym. Sci.* **7**, 873 (1963).
3. A.R. Payne, *J. Appl. Polym. Sci.* **9**, 2273, 3245 (1965).
4. A.R. Payne, *J. Appl. Polym. Sci.* **11**, 383 (1967).
5. T.A. Witten, M. Rubinstein and R.H. Colby, *J. Phys. II France* **3**, 367 (1993).
6. G. Huber, T.A. Vilgis and G. Heinrich, *J. Phys.: Condens. Matter* **8**, L409 (1996).
7. G. Huber and T.A. Vilgis, *Kautsch. Gummi Kunstst.* **52**, 102 (1999).
8. S. Vieweg, R. Unger, G. Heinrich and E. Donth, *J. Appl. Polym. Sci.* **73**, 495 (1999).
9. N.K. Dutta, D. Khastgir and D.L. Tripathy, *J. Mater. Sci.* **26**, 177 (1991).
10. K. Mukhopadhyay, D.K. Tripathy and S.K. De, *J. Appl. Polym. Sci.* **48**, 1089 (1993).
11. C.R. Lin and Y.D. Lee, *Macromol. Theory Simul.* **5**, 1075 (1996).
12. J.D. Ulmer, *Rubber Chem. Technol.* **69**, 15 (1996).
13. A. Lion, *J. Mech. Phys. Solids* **45**, 1805 (1997).
14. A. Lion, *J. Mech. Phys. Solids* **46**, 895 (1998).
15. A.K. Manna, P.P. De, D.K. Tripathy and S.K. De, *J. Appl. Polym. Sci.* **70**, 723 (1998).
16. L. Chazeau, J.D. Brown, L.C. Yanyo and S.S. Sternstein, *Polym. Comp.* **21**, 202 (2000).
17. G. Kraus, *J. Appl. Polym. Sci., Appl. Polym. Symp.* **39**, 75 (1984).
18. F. Carmona, *Physica A* **157**, 461 (1989).
19. F. Lux, *J. Mater. Sci.* **28**, 285 (1993).
20. L. Karasek and M. Sumita, *J. Mater. Sci.* **31**, 281 (1996).
21. M.S. Green and A.V. Tobolsky, *J. Chem. Phys.* **14**, 80 (1946).
22. M. Yamamoto, *J. Phys. Soc. Japan* **11**, 413 (1956).
23. A.S. Lodge, *Rheol. Acta* **7**, 379 (1968).
24. F. Tanaka and S.F. Edwards, *Macromolecules* **25**, 1516 (1992).
25. J.L. Lablanc, *J. Appl. Polym. Sci.* **66**, 2257 (1999).
26. A. Medalia, *J. Colloid Interface Sci.* **32**, 115 (1970).
27. B. Wessling, *Synth. Met.* **28**, C849 (1989).
28. A.D. Drozdov, *Mechanics of Viscoelastic Solids* (Wiley, Chichester, 1998).
29. M. Doi and S.F. Edwards, *The Theory of Polymer Dynamics* (Oxford University Press, Oxford, 1986).
30. L. Mullins and N.R. Tobin, *J. Appl. Polym. Sci.* **9**, 2993 (1965).

31. E. van der Giessen, *Eur. J. Mech. A/Solids* **16**, 87 (1997).
32. F.W. Starr, T.B. Schroder and S.C. Glotzer, preprint cond-mat/0007486.
33. L.R.G. Treloar, *The Physics of Rubber Elasticity* (Clarendon Press, Oxford, 1975).
34. G.E. Pike and C.H. Seager, *Phys. Rev. B* **10**, 1421, 1435 (1974).
35. J.P. Straley, in *Electrical Transport and Optical Properties of Inhomogeneous Media*, Eds. J.C. Garland and D.B. Tunner (AIP, New York, 1978), p. 118.
36. J.J. Cai and R. Salovey, *J. Mater. Sci.* **34**, 4719 (1999).
37. L. Flandin, J.-Y. Cavaille, Y. Brechet and R. Dendievel, *J. Mater. Sci.* **34**, 1753 (1999).
38. L. Flandin, A. Hiltner and E. Baer, *Polymer* **42**, 827 (2001).



## FIGURES

Fig. 1. The storage modulus  $E'$  MPa versus the frequency of oscillations  $\omega$  Hz for CB filled natural rubber in a tensile dynamic test with the strain amplitude  $\Delta$  at a temperature  $T$  K. Circles: experimental data<sup>14</sup>. Solid lines: results of numerical simulation. A:  $T = 253$ ; B:  $T = 296$ ; C:  $T = 333$ ; D:  $T = 373$ . Curve 1:  $\Delta = 0.006$ ; curve 2:  $\Delta = 0.011$ ; curve 3:  $\Delta = 0.028$ ; curve 4:  $\Delta = 0.056$

Fig. 2. A: The elastic modulus  $K$  versus the amplitude of oscillations  $\Delta$  at a temperature  $T$  K. Solid lines: approximation of the experimental data by Eq. (21). Curve 1:  $T = 253$ ,  $a_0 = 7.2672$ ,  $a_1 = 5.3129$ ; curve 2:  $T = 296$ ,  $a_0 = 4.6737$ ,  $a_1 = 3.4019$ ; curve 3:  $T = 333$ ,  $a_0 = 3.0929$ ,  $a_1 = 2.5039$ ; curve 4:  $T = 373$ ,  $a_0 = 2.8935$ ,  $a_1 = 1.9944$ . B: The standard deviation of the number of strands  $\Sigma$  (unfilled circles) and the initial modulus  $K(0)$  (filled circles) versus the degree of undercooling  $\Delta T$  K. Solid lines: approximation of the experimental data by Eq. (22). Curve 1:  $b_0 = 2.0465$ ,  $b_1 = 16.246$ ; curve 2:  $c_0 = 1.7553$ ,  $c_1 = 185.33$ . C: The rate of breakage  $\Gamma_0$  s<sup>-1</sup> versus the degree of undercooling  $\Delta T$  K. Solid line: approximation of the experimental data by Eq. (23) with  $d_0 = -0.9827$  and  $d_1 = 9.3009 \times 10^{-2}$ . D: The coefficient  $\kappa$  versus the degree of undercooling  $\Delta T$  K. Solid line: the average value  $\kappa = 5.7$ . Symbols: treatment of observations for CB filled natural rubber<sup>14</sup>

Fig. 3. The storage modulus  $E'$  MPa versus the frequency of oscillations  $\omega$  Hz for CB filled bromobutyl rubber in a tensile dynamic test with the strain amplitude  $\Delta$  at room temperature. A:  $\phi = 30$ ; B:  $\phi = 50$ ; C:  $\phi = 70$ ; D:  $\phi = 100$ . Circles: experimental data<sup>9</sup>. Solid lines: results of numerical simulation. Curve 1:  $\Delta = 0.0003$ ; curve 2:  $\Delta = 0.0011$ ; curve 3:  $\Delta = 0.0033$ ; curve 4:  $\Delta = 0.0048$ ; curve 5:  $\Delta = 0.0077$ ; curve 6:  $\Delta = 0.0122$

Fig. 4. The standard deviation of the number of strands  $\Sigma$  and the elastic modulus  $K$  MPa versus the amplitude of oscillations  $\Delta$  for CB filled bromobutyl rubber. Circles: treatment of observations<sup>9</sup>. Solid lines: approximation of experimental data by Eq. (24). A:  $\phi = 30$ , Curves 1:  $A_0 = 0.6474$ ,  $A_1 = 0.1208$ ;  $B_0 = 10.0943$ ,  $B_1 = 1.5797$ ; B:  $\phi = 50$ , Curves 1:  $A_0 = 0.9702$ ,  $A_1 = 0.0084$ ,  $B_0 = 8.4060$ ,  $B_1 = 0.7724$ , curves 2:  $A_0 = -0.1828$ ,  $A_1 = 0.4658$ ,  $B_0 = 42.2894$ ,  $B_1 = 14.5677$ ; C:  $\phi = 70$ , Curve 1:  $B_0 = 3.7590$ ,  $B_1 = -0.0458$ , curves 2:  $A_0 = -0.0706$ ,  $A_1 = 0.3871$ ,  $B_0 = 44.4787$ ,  $B_1 = 14.4917$ ; D:  $\phi = 100$ ; Curve 1:  $B_0 = 2.8452$ ,  $B_1 = -0.7079$ ; curves 2:  $A_0 = 0.1749$ ,  $A_1 = 0.2567$ ;  $B_0 = 39.7411$ ,  $B_1 = 11.5563$

Fig. 5. A: The parameters  $A_0$  (unfilled circles) and  $A_1$  (filled circles) versus the degree of loading  $\phi$  phr. Solid lines: approximation of the experimental data by Eq. (25). Curve 1:  $A_{00} = -0.5568$ ,  $A_{01} = 7.2353 \times 10^{-3}$ ; curve 2:  $A_{10} = 0.6775$ ,  $A_{11} = 4.1950 \times 10^{-3}$ . B: The parameters  $B_0$  (unfilled circles) and  $B_1$  (filled circles) versus  $\phi$  phr. Solid lines: approximation of the experimental data by Eq. (26). Curve 1:  $B_{00} = 13.3942$ ,  $B_{01} = 0.1059$ ; curve 2:  $B_{10} = 2.4530$ ,  $B_{11} = 0.0329$ . C: The critical amplitude of oscillations  $\Delta\epsilon_{cr}$  versus  $\phi$  phr. Solid line: approximation of the experimental data by Eq. (27) with  $C = 1.4711 \times 10^{-2}$ ,  $\beta = 0.6616$  and  $\phi_{cr} = 40.99$  phr. D: The parameter  $\kappa$  versus  $\phi$  phr. Solid line: the limiting value  $\kappa = 16.0$ . Symbols: treatment of observations for CB filled bromobutyl rubber at room temperature<sup>9</sup>

Fig. 6. A and B: The storage modulus  $E'$  MPa versus the frequency of oscillations  $\omega$  Hz for CB filled bromobutyl rubber in a tensile dynamic test with the strain amplitude  $\Delta = 0.01$  at a temperature  $T$  °C. Symbols: experimental data<sup>9</sup>. Solid lines: results of numerical simulation. A:  $\phi = 60$  phr, B:  $\phi = 100$  phr. Curves 1:  $T = 25$ ; curves 2:  $T = 50$ ; curves 3:  $T = 100$ . C: The standard deviation of the number of strands  $\Sigma$  versus the degree of undercooling  $\Delta T$  K. Symbols: treatment of observations. Solid lines: approximation of the experimental data by Eq. (22). Curve 1:  $\phi = 60$  phr,  $b_0 = 0.6956$ ,  $b_1 = -8.8493$ ; curve 2:  $\phi = 100$  phr,  $b_0 = 0.5400$ ,  $b_1 = -18.337$ . D: The elastic modulus  $K$  MPa versus the degree of undercooling  $\Delta T$  K. Symbols: treatment of observations. Solid lines: approximation of the experimental data by Eq. (22). Curve 1:  $\phi = 60$  phr,  $c_0 = 14.084$ ,  $c_1 = -236.96$ ; curve 2:  $\phi = 100$  phr,  $c_0 = 24.086$ ,  $c_1 = -911.59$

Fig. 7. A and B: The storage modulus  $E'$  MPa versus the frequency of oscillations  $\omega$  rad/s for filled styrene-butadiene rubber (SBR-1500) with a degree of loading  $\phi$  phr in a tensile dynamic test with the strain amplitude  $\Delta = 0.002$  at the temperature  $T = -30$  °C. A: CB filled elastomer; B: polymeric filled elastomer. Circles: experimental data<sup>8</sup>. Solid lines: results of numerical simulation. Curve 1:  $\phi = 0$ ; curve 2:  $\phi = 25$ ; curve 3:  $\phi = 50$ ; curve 4:  $\phi = 75$ ; curve 5:  $\phi = 100$ . C: The standard deviation of the number of strands  $\Sigma$  versus the degree of loading  $\phi$  phr. Solid lines: approximation of the experimental data by Eq. (28). Curve 1a:  $C_0 = 1.0864$ ,  $C_1 = -0.0013$ ; curve 2a:  $C_0 = 0.7832$ ,  $C_1 = 0.0063$ ; curve 1b:  $C_0 = 1.0864$ ,  $C_1 = -0.0010$ ; curve 2b:  $C_0 = 0.9003$ ,  $C_1 = 0.0071$ . D: The elastic modulus  $K$  MPa versus  $\phi$  phr. Solid lines: approximation of the experimental data by Eq. (28). Curve 1a:  $D_0 = 3.8947$ ,  $D_1 = -0.0211$ ; curve 2a:  $D_0 = 4.8175$ ,  $D_1 = 0.0064$ ; curve 1b:  $D_0 = 3.8947$ ,  $D_1 = -0.0097$ ; curve 2b:  $D_0 = 4.2435$ ,  $D_1 = 0.0055$ . Symbols: treatment of observations<sup>8</sup>. Unfilled circles: CB filler; filled circles: polymeric filler

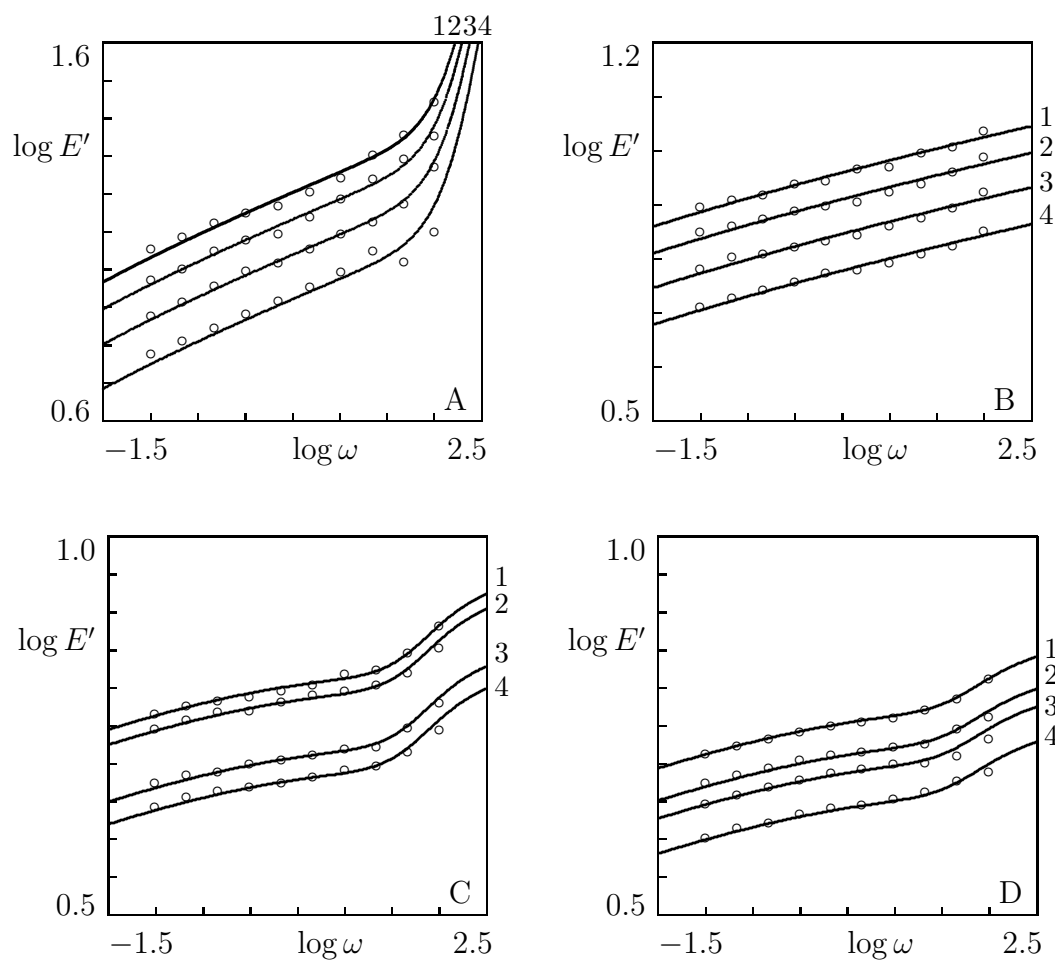


Fig. 1.

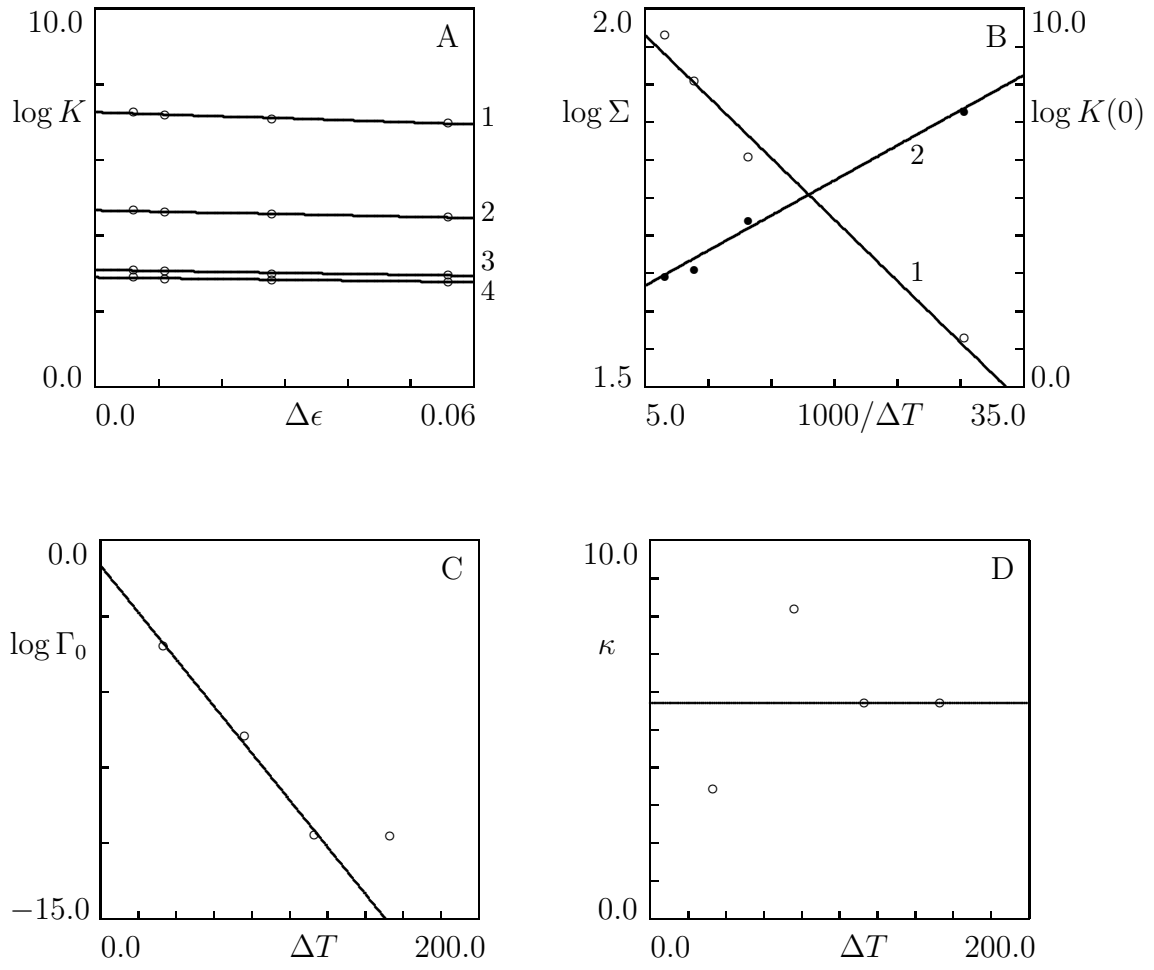


Fig. 2.

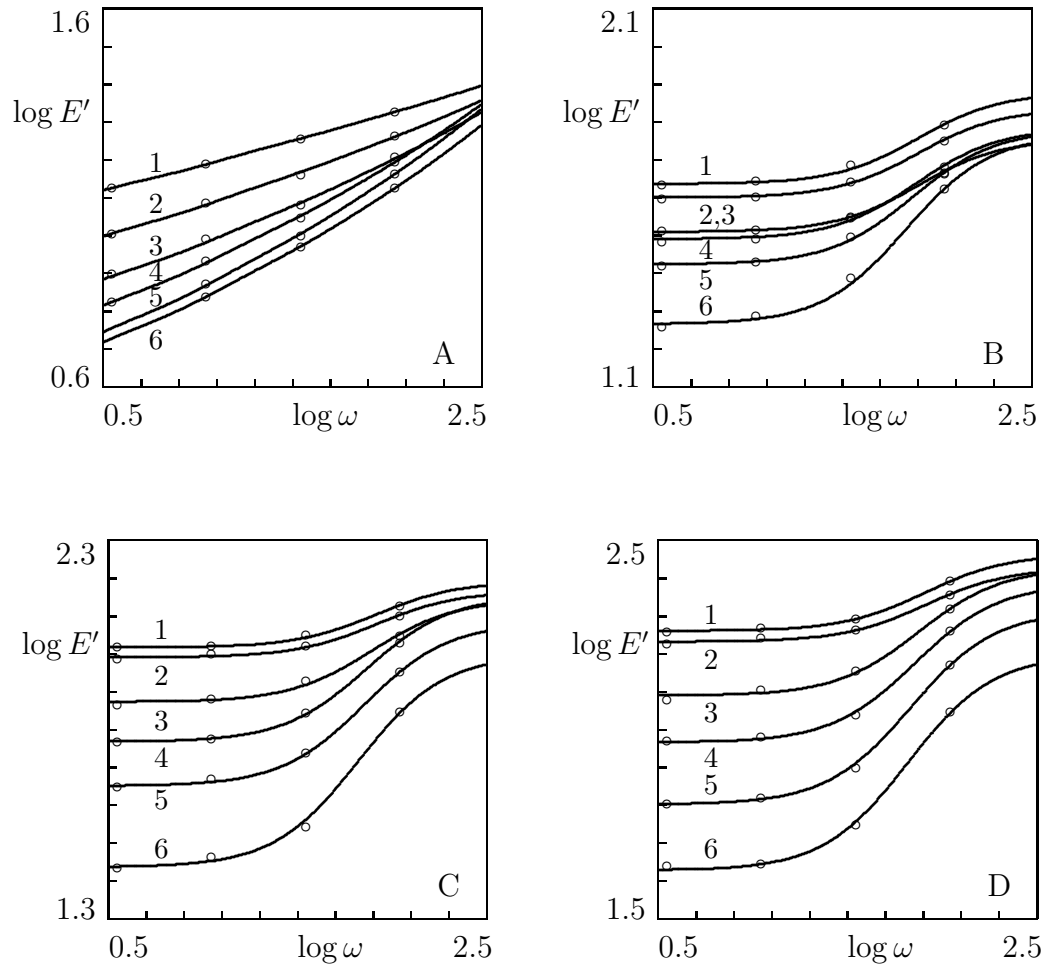


Fig. 3.

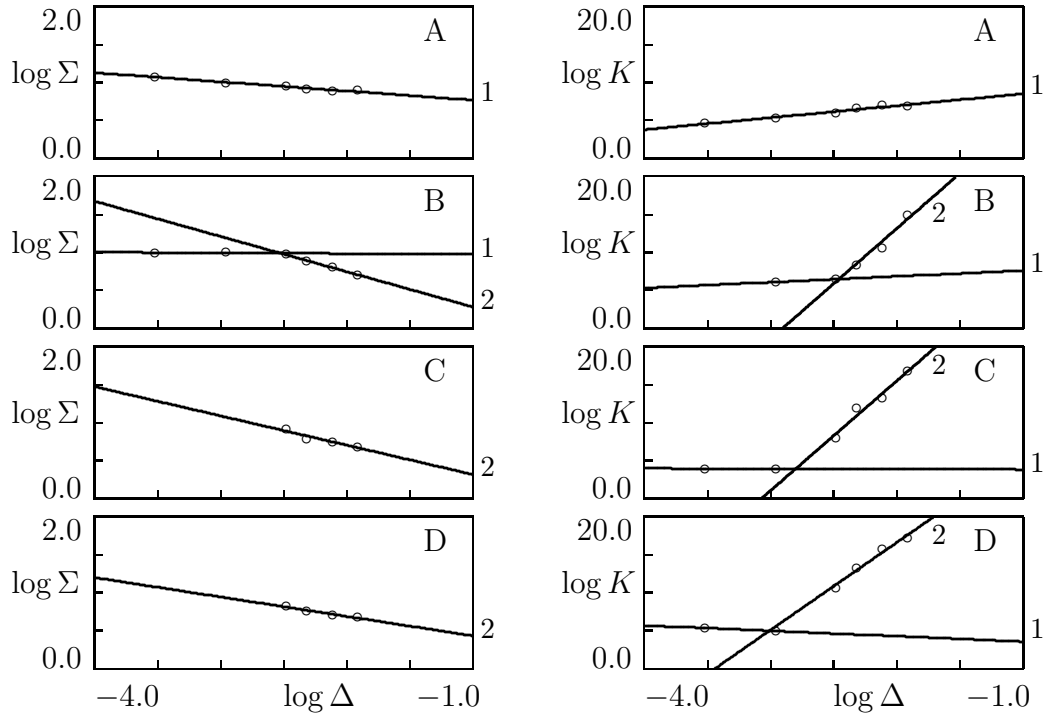


Fig. 4.

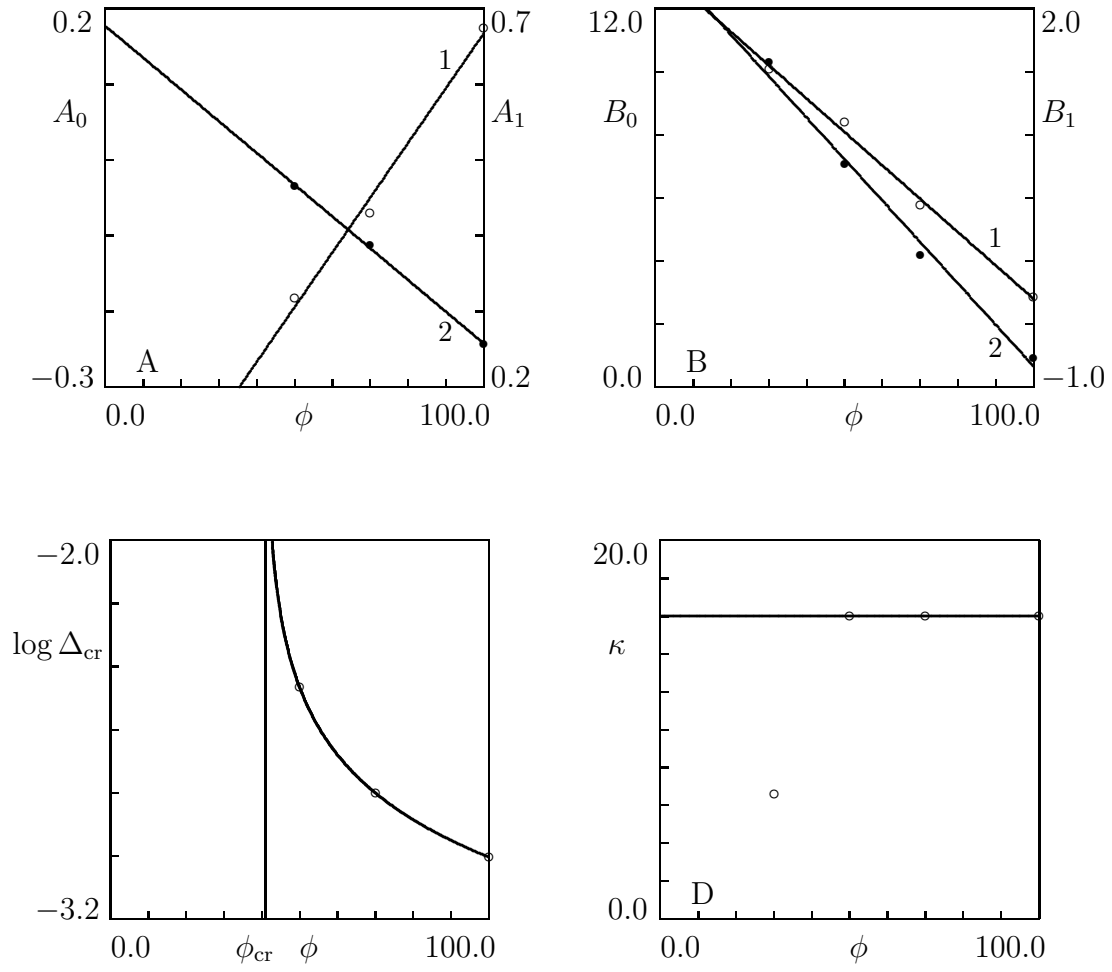


Fig. 5.



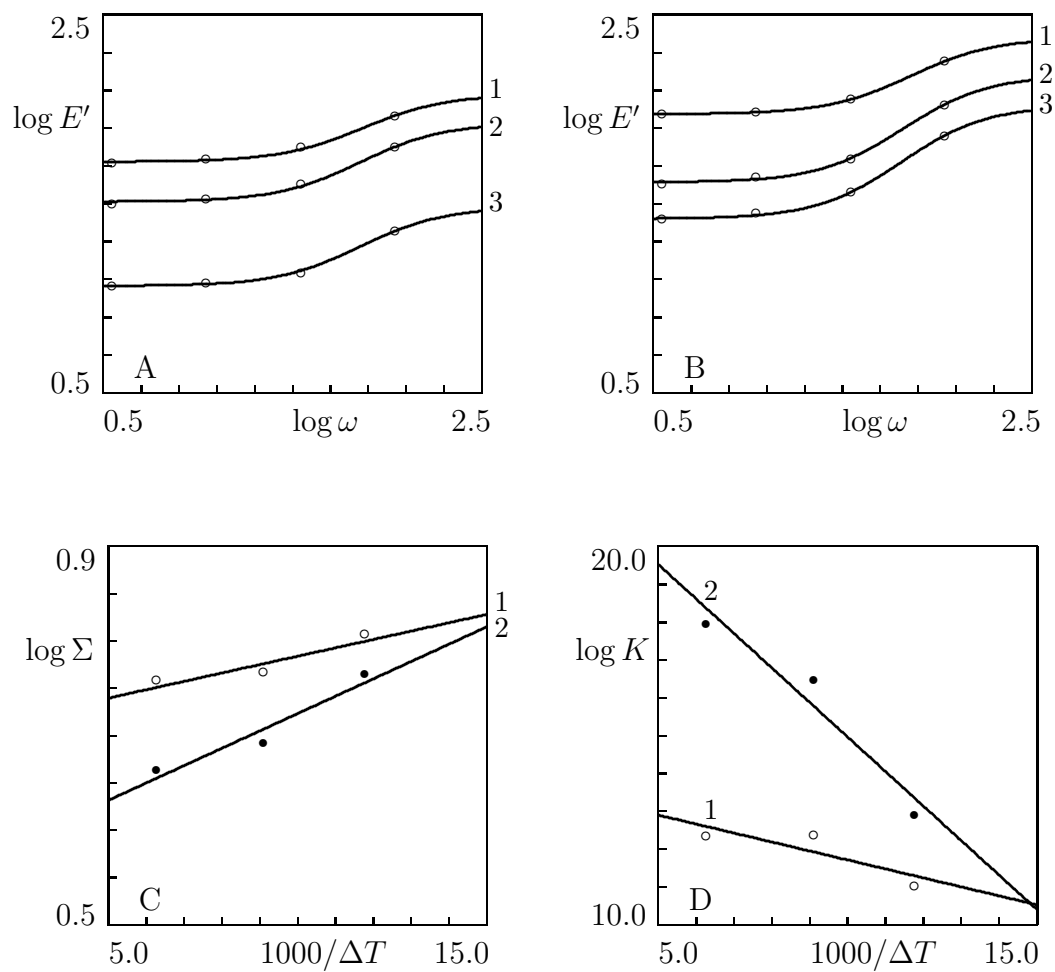


Fig. 6.

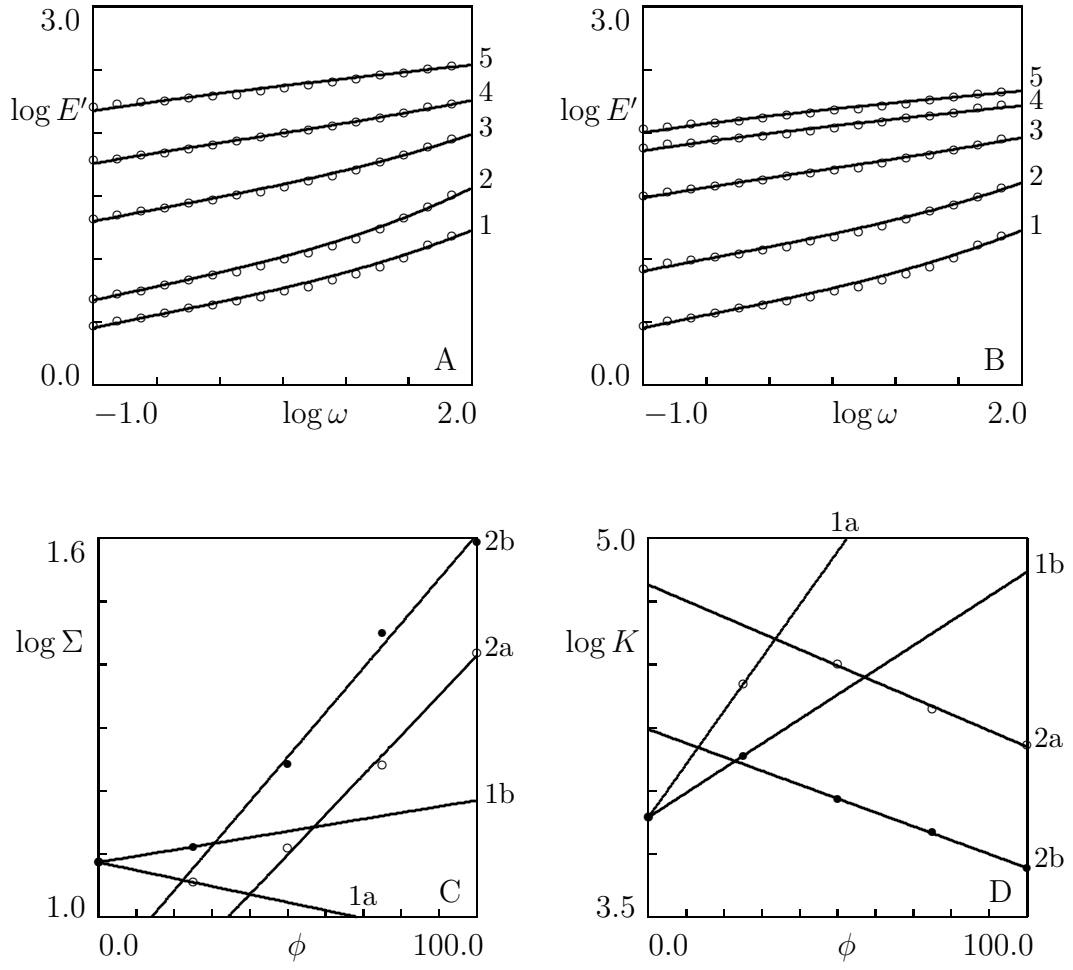


Fig. 7.